ESTIMATING THE SPATIAL DISTRIBUTION OF
SNOW WATER EQUIVALENCE IN A MONTANE WATERSHED

Kelly Elder †,   Walter Rosenthal ††,   Bert Davis ‡

ABSTRACT

We describe an approach to model distributed snow water equivalence (SWE) that merges field measurements of depth and density with remotely sensed snow-covered area (SCA). In 1993 two teams conducted an intensive snow survey in the $92.8\,km^2$ Blackcap Basin of the Kings River. We measured snow depth at 709 points and density in five snow pits and along five transects using a Federal Sampler. Sample locations were chosen to be representative of the range of elevations, slopes and aspects of the basin. Regression tree models showed that net radiation, elevation, and slope angle account for 60-70% of the variance in the depth measurements. Density was distributed over the basin on a $30\,m$ grid with a multiple linear regression model that explained 70% of the observed variance as a function of the same three variables. The gridded depth estimates combined with modeled density produced spatially distributed estimates of SWE. An unsupervised spectral unmixing algorithm estimated snow cover fractions from Landsat-5 Thematic Mapper data acquired at the time of the snow survey. This method provides a snow cover fraction estimate for every pixel. We used this subpixel map as our best estimate for SCA and combining it with the SWE map allowed us to compute SWE volume. We compared the estimated volume using the subpixel SCA map with several SCA maps produced with simulations of binary SCA mapping techniques. Thresholds of 40%, 50% and 60% fractional cover were used to map binary cases of full snow cover or no snow cover. The difference in basin SWE volume was up to 13% depending on the threshold used to classify snow-covered versus snow-free areas. The percent differences in volumes roughly corresponded to the percent differences in SCA between the methods.

INTRODUCTION

In watersheds where melting snow produces much of the annual runoff, the most important variable to hydrologic forecasters is the total volume of water stored in the form of snow. In the western U.S., for example, information on snow cover has become critical as many interests compete for the variable water supply. As snow melt modeling and forecasting tools become more complex, the spatial distribution of snow water equivalence (SWE) has increased in importance. Information on the spatial distribution is critical to accurate forecasting of both total volume and timing of the runoff. Operational efforts (e.g., Carroll, 1995; Carroll and Cressie, 1996) and research efforts (e.g., Elder et al., 1991 and 1995; Hosang and Dettwiler, 1991; Elder, 1995) to map SWE utilizing remotely sensed data to interpolate point and transect measurements have progressed rapidly in recent years, providing information in data-sparse regions. Spatial models developed for operational purposes use standard network data from snow courses, SNOTEL sites and aircraft flight lines (Carroll et al., 1995), while research efforts have had the benefit of comprehensive outcome-based snow surveys.

Snow-covered area (SCA) can be measured with a variety of methods, such as aerial photography and satellite imagery, but operational measurements of SWE in montane areas are still ground based. Measuring SWE with airborne techniques, such as gamma-ray attenuation along flight lines, or satellite techniques, such as active and passive microwave backscatter, either are not suitable or have not been sufficiently developed for operational observation of deep snow cover in rugged mountain terrain. This void has motivated recent research to use land cover, terrain and other information to model the distribution of SWE. When snow cover in a basin or modeling area is discontinuous, the total SWE is more sensitive to the SCA than to the average snow depth. Therefore, interpolations of SWE are commonly adjusted with maps of snow-covered area, of which there are two types.

†Department of Earth Resources, Colorado State University, Fort Collins, CO 80523, Tel: 970-491-5454,
    Email: kelder@cnr.colostate.edu
††Institute for Computational Earth System Science, University of California, Santa Barbara, CA 93106,
    Tel: 619-935-4464, Email: walter@icess.ucsb.edu
‡Cold Regions Research and Engineering Laboratory, 72 Lyme Road, Hanover, NH 03755, Tel: 603-646-4219,
    Email: bert@crrel41.crrel.usace.army.mil

Binary mapping is the process where one or more thresholds determine whether a pixel will be assigned a snow cover of 100% or 0%. Visible and near-infrared sensors have been used extensively to delineate areas of snow cover using both supervised (e.g., Dozier, 1984; Maxson et al., 1996), and unsupervised binary classification (e.g., Dozier, 1989; Hall et al., 1995 and 1996). This type of snow map provides information on the snow boundary, providing SWE interpolation techniques the locations of pixels where SWE equals 0. Errors in SWE estimation using binary maps derive from the interpolation scheme within the snow-covered area. For point measurement sites, snow and no-snow classes represent 100% and 0% snow, respectively. However, at resolutions of commercial satellite sensors, many pixels may contain a mixture of snow-covered and bare areas. Thus, while point-like data would describe the true distribution of snow cover, pixels from most sensors describe some threshold class on the probability density function (PDF) of snow cover fractions. Interpolations of SWE in this case are adjusted by removing snow from all snow-covered pixels below the binary threshold, while snow-free pixels above the binary threshold will be assigned some SWE value. The net error is small if the PDF has a symmetric distribution around the mapping threshold at all scales, from individual pixels to cumulative totals over larger areas.

In contrast, recent investigations have used spectral mixture analysis to estimate snow cover fractions on a pixel-by-pixel basis (Nolin and Dozier, 1993; Painter et al., 1996; Rosenthal and Dozier, 1996; Rosenthal, 1996a and 1996b). The spectrum of each pixel is assumed to be comprised of area-weighted contributions of pure component or endmember spectra (pure snow, rock, vegetation, etc.). Spectral mixture analysis estimates the areal fractions of scene endmembers in each pixel, plus an error term describing the performance of the mixture model for each pixel. Snow area-fraction maps offer the opportunity to adjust SWE interpolations on a pixel basis. The preliminary estimate of SWE can be multiplied by the snow area in each pixel to yield the total water equivalent volume.

In this paper we examine different methods for interpolating SWE and the impact on SWE estimates of mapping SCA with the two methods.

STUDY SITE

The Blackcap Basin is a headwater catchment of the North Fork of the Kings River, within the Sacramento River basin of California (Figure 1). It covers 9280 ha, and ranges in elevation from 2476 m at the Beaver Meadows stream gauge to 3827 m at the summit of Mt. Goddard. The average slope derived from the USGS 30 m DEM is 16°, with a general west northwest drainage towards the Pacific Ocean. Alpine cirques and dense forest cover substantial portions of the basin, which constitute similar proportions of the seasonally snow-covered Kings River basin.

FIELD WORK

Field work was conducted in the basin from 5 to 7 May, 1993. Two teams measured snow depth with aluminum probes and dug snow pits to measure snow density. Depth transects and snow pits were located using portable GPS units so the data could later be registered to a 30 m USGS DEM. Figure 2 shows the basin with the location of the depth transects and snow pits.

One team remained in the alpine zone, making about 400 depth measurements and excavating four snow pits on a variety of representative aspects, elevations, and slopes. Depths were taken along transects with 10 and 20 m resolutions.

The second team worked primarily below treeline, taking over 300 depth measurements, 155 SWE measurements with a Federal (Mount Rose) Sampler, and digging two snow pits. Federal Sampler measurements were calibrated against snow density estimates from the pits. Depths were measured at 10 m intervals along six transects selected for differences in vegetation cover, aspect and elevation. The selection of the transect locations is subjective and biases the results of the study, but such decisions must be made when surveying large basins with limited time and personnel. Federal Sampler measurements were taken at the beginning, end, and at 100 m intervals along four of the transects. Each set of 5 Federal Sampler measurements was made in a "+" pattern, with cores at a central point and 5 m away in four directions. The mean of each set was taken to represent the local SWE. The first, last, and central points of the Federal Sampler transects were located with a portable GPS unit. A single Federal Sampler transect was taken at an elevation of 3230 m.

1993 SNOWPACK CONDITIONS

Seasonal precipitation for the state on May 1 was estimated to be 143% of the 50 year average (California Cooperative Snow Surveys, 1993). Precipitation over the Tulare Basin (which includes the Kings River and Blackcap Basin) was estimated to be 134% of the 1 May average, while SNOTEL sites indicated a mean of 0.85 m of water basin-wide, 140% of the 1 May average. Unimpaired runoff from the Kings River drainage was forecast at 150 percent of the April-July normal discharge.

The upper Blackcap Basin was sampled before substantial snow loss occurred from melt. Snow pit temperature profiles showed that the cold content had not yet been entirely removed at elevations between 3300 and 3500 m, with temperatures of some strata being near -1°C.

The lower portions of the basin had experienced considerable melt and runoff by the time the field work began. Discharge in the streams was relatively high, overland flow was observed on almost all snow-free slopes, and ponding was observed in hollows not easily drained. In the lowest portions of the basin, large expanses of granite slab and unforested terrain were snow-free on south-facing slopes.

MODELING METHODS

The goal of the SWE modeling portion of the study was to distribute SWE over all snow-covered portions of the basin as accurately as possible. Snow depth and density, the two components of SWE at a point, had to be spatially interpolated over the basin.

Snow Depth

Snow depth exhibits great spatial variability in montane basins and a long-standing question in snow hydrology has been how best to distribute point measurements of snow depth over complex terrain. The approach we have used employs the relatively new statistical technique of binary decision trees (Breiman et al., 1984; Clark and Pregibon, 1992). The technique has been shown to produce satisfactory results in a small alpine basin (Elder, 1995; Elder et al., 1995). The current study used the S-Plus mathematical language (Chambers and Hastie, 1992) to construct the regression models (Clark and Pregibon, 1992).

Co-registered independent variables, paired with the dependent variable, form a learning sample set for the regression tree model. Regression trees are constructed by sequentially dividing the data set into binary groups using all binary possibilities and all independent variables. The split that maximizes the reduction in total tree deviance is the split chosen for a given data group or node. Each descendant node is then repeatedly split in the same fashion. Continued splits resulting in the same number of nodes as data points are possible, but give a statistically and physically unreal model of the data. Typically, regression tree algorithms overfit the data, then prune the resultant tree back to a statistically defensible size. Once an acceptable tree is grown and pruned using the learning set, the tree can be used to predict the dependent variable (in this case snow depth) over space using the full set of independent variables. The reader is referred to Breiman et al. (1984) for a comprehensive discussion of regression trees.

In this study, the independent variables used to model snow depth were calculated net radiation, elevation and slope. Potential net solar radiation was calculated using the algorithm of Dozier (1980) as implemented in IPW software (Frew and Dozier, 1986) and using atmospheric parameters derived from LOWTRAN7 (Kneizys et al., 1988). Daily values were calculated for each pixel in the basin for the 15th of each month from December through April. The cumulative value for the five dates was used as an index of net solar radiation. Elevation and slope were derived directly from a 30 m USGS digital elevation model of the basin. All spatial modeling was carried out at the 30 m grid scale using the GRASS GIS where co-registered data layers of net radiation, elevation and slope were constructed for the entire basin. Figures 3 through 5 show digital maps of net radiation, elevation and slope, respectively.

The overfit snow depth tree was pruned to 25 nodes based on cross validation results and the coefficient of determination. The 25-node tree with the decision splits and terminal node SWE values is plotted in Figure 6. The tree model was then used to construct a spatial map of snow depth for each 30 m pixel in the basin as shown in Figure 7.

Snow Density

Snow density is conservative in comparison to depth, particularly after the snowpack has ripened (Elder et al., 1991). Therefore, fewer measurements of density are required than of depth. Density values were derived by two methods. Where Mt. Rose measurements were taken along a depth transect, the mean density was assigned to the midpoint of the transect. Where snow pits were excavated and density profiles obtained, the weighted mean density from the pit was assigned to the pit location. Five snow pit and five transect mean densities were used to distribute density over the basin. A simple linear model was applied to the point values of snow density from the pits and transects. Independent variables used to estimate density were net solar radiation, elevation and slope. Calculated net radiation and elevation were used because both are physically based parameters that control the energy balance at a point in the basin, and therefore, snow metamorphism and ultimately snow density. Slope relates to density through redistribution of snow via avalanching and wind transport.

The simple linear model explained 70% of the observed variance in the field measurements of density ($R^2 = 0.70$, n = 10, p = 0.054), although the aggregation of the transect data tends to produce an optimistic fit. Figure 8 shows the distributed density over the basin. Note the similarity between the distributed density of Figure 8 and calculated net radiation in Figure 3. The strong correlation should not come as a surprise because the energy balance of the snowpack controls metamorphism and densification, and the snowpack energy balance is dominated by radiation in this environment.

Snow-Covered Area

Most algorithms for estimating SCA from multispectral satellite data are binary: pixels are classified either snow-covered or snow-free. (Rango and Itten, 1976; Martinec and Rango, 1981; Dozier and Marks, 1987; Dozier, 1989; Hall et al., 1995). Most pixels, however, are mixtures of snow, rock, vegetation, or water. Rosenthal and Dozier (1996) used a decision tree model (Breiman et al., 1984; Clark and Pregibon, 1992) to generalize spectral mixture analyses of reference Thematic Mapper (TM) data and accurately map snow cover in the Sierra Nevada at subpixel resolution. In spectral mixture analysis, the measured pixel spectrum is modeled as a linear combination of endmember spectra. The method was first used to identify components in chemical mixtures (Lawton and Sylvestre, 1971), but has been widely applied in the Earth and planetary sciences. For example, it has been used to map regional vegetation and geologic substrates (Smith et al., 1990), and estimate suspended sediment concentrations in the Amazon River (Mertes et al., 1993).

Direct, supervised spectral unmixing is an iterative, subjective, and time-consuming process, since endmember combinations may number in the hundreds of thousands. An unsupervised approach using convex hull geometry was described by Boardman (1993). Rosenthal (1996) developed an automated approach for mapping alpine snow cover at subpixel resolution from TM data that provides SCA estimates comparable to those obtainable from aerial photographs.

We used this method for mapping fractional SCA in a TM scene acquired on 13 May, 1993, and briefly summarize it here. The decision tree program from Rosenthal and Dozier (1996) masked clouds and separated snow-free pixels from those probably containing snow. Snow pixels were further sorted into sets of pixels suffering from detector saturation in at least one band, and those free of saturation problems.

For each of these image fragments the dimensionality of the data D was estimated by principal components analysis. The best set of $k = D + 1$ image endmembers was assumed to lie on the convex hull of the data, and the n points on the D-dimensional convex hull were identified.

The number of sets of size k that can be drawn from a set of n points (C_k^n) is

$$C_k^n = \frac{n!}{(n-k)!k!}$$

All C_k^n mixture models (60152) were computed using singular value decomposition, with the endmember fractions constrained to be non-negative and to sum to 1 or less. The models were ranked by RMSE and the model with the lowest value was chosen as the "best".

The endmembers for each image fragment were identified and converted to surface reflectance using the 5S radiative transfer code (Tanré et al., 1990). The best matches to the corrected endmember reflectance spectra were found by automated search of a spectral library. The search method computed the error sum of squares between endmember and library spectra (Lowry and Huppler, 1981), and used a library drawn primarily from Satterwhite

and Henley, 1990. The purity of the snow endmembers was estimated by unmixing them as linear combinations of spectra from the convex hull of the entire data set. We then modeled the full scene with the best endmember set from each image fragment, and the model with the smallest RMSE was chosen for each pixel. The raw snow fractions were weighted by the snow purity estimates, and the sum of all snow fractions was divided by the sum of all endmember fractions for each pixel to produce the final fractional snow cover map.

RESULTS

Snow Depth

Qualitative assessment of the snow depth model fit can be made by noting that the snow is deepest at high elevation, northerly-facing locations. Lowest accumulations are located at low elevations with southerly aspects. Inspection of the 25-node tree (Figure 6) also gives credence to reasonable model representation of physical processes. The first split is made on elevation at a relatively low value on the basin. This split separates the low valley bottom from the remaining basin. The next split is on net radiation and as one would expect, higher radiation values result in lower snow accumulations. This relationship between radiation and snow depth is fairly consistent throughout the tree. Slope plays a less important role than radiation or elevation, but accumulations are generally greater on slopes of less than 37°. We expect this result because steeper slopes avalanche more frequently, reducing accumulation.

To obtain a more quantitative assessment of model fit, the full-sized tree was pruned one node at a time and the volume of SWE and the coefficient of determination were calculated for each tree. The coefficient of determination was calculated using standard statistical procedures (Zar, 1978), where the modeled depth was compared with the measured depth for co-registered locations of all 709 field data points (Figure 9). The graph shows a rapid increase in fit as the number of terminal nodes or snow depth classes is increased, with an asymptotic approach to the 0.70 value. The 7-node tree explains 50% of the observed variance in snow depth and the 13-node tree explains 60%. The 30-node tree explains 70% of the observed variance, while the 25-node tree suggested by cross validation explains only slightly less at 68%. There is improvement in model performance with increased model complexity after 25 nodes. We recognize that this measure of model performance ignores spatial autocorrelation of the measured depths, but it is a relative indicator of goodness of fit. The autocorrelation problem suggests that the R^2 values are overestimates to some degree.

Snow-Covered Area

Figure 10 shows the subpixel fraction map of SCA. We were interested in comparing the estimated SCA from the subpixel method with a standard binary mapping algorithm. To simulate a binary snow mapper, we applied three thresholds to the subpixel snow map, effectively turning it into binary maps with differing detection limits. The first binary map was constructed by assigning 100% snow cover to any pixel with 40% or more snow cover, and simulates an algorithm that overestimates a binary snow distribution. The second case assigned 100% cover to all pixels with 50% or more cover, and represents a best-case algorithm. The last map assigned 100% snow cover to all pixels with 60% or greater snow cover, representing a binary mapper that underestimates SCA. All three maps are shown in Figure 11.

The different methods of classifying snow-covered area produced significantly different areal estimates. Table 1 summarizes SCA values in terms of actual areal cover and percent of the total basin area. In addition, the differences between the subpixel method and the three binary mappings are shown, where positive values are overestimates of the subpixel SCA estimate. The subpixel estimate was determined by multiplying each pixel area by the percent of the pixel determined to be snow covered and summing over the entire basin. The subpixel method produced a total SCA of 7660 ha, or 82.6% of the basin area. The binary estimates were determined by simply counting the number of pixels that were snow covered and multiplying by the pixel area. The binary methods ranged from an overestimate of 13.3% using the 40% threshold, to an underestimate of 3.4% with the 60% threshold (Table 1).

Snow Water Equivalence

SWE volume was calculated by multiplying the modeled depth by the modeled density and the SCA fraction for each pixel, then summing over the basin to obtain the total volume shown in Figure 12. The binary SCA maps considered predicted SWE only in pixels containing snow.

The difference between the subpixel and the 40% binary mappers in predicted SWE volume is similar to the differences in estimated SCA, with an estimated volume difference of 13% (Table 2). The differences between the subpixel and 50% and 60% snow mappers depart from the relative differences in the SCA analysis above, indicating that the distributions of both the water equivalent and the snow cover are changing.

DISCUSSION

This paper presented a conservative example of the sensitivity of total basin SWE to different variables. We focused on the spatial distribution of SWE: depth and SCA were the two primary factors of interest. The qualitative and quantitative assessments of snow depth modeling using binary regression trees indicate that the method works well. The density model we chose was one of a number of possibilities that could have been applied. However, different techniques for distributing density in the basin would have produced little change in the results because there was little observed spatial variability in this parameter. The measurements were taken after the most of the snowpack in the basin had ripened, so density was conservative compared to depth. The test basin is largely above tree line, and the field work was carried out at a date close to peak accumulation. Both of these factors lead to a spatial distribution of SCA that produces large areas of nearly 100% snow cover. Figure 13 shows the percentage of the basin's total pixel coverage (area) that belong to a given fractional snow cover. This histogram shows that more than 65% of the basin shows pixels with greater than 90% snow cover; more than 85% of the basin has snow cover exceeding 50%. This uniform cover allows a binary SCA classifier to produce accurate results because few pixels are near the threshold where the classifier has trouble making the distinction between snow-covered and snow-free area. Hall et al. (1996) showed similar results using imagery over the same general region at approximately the same time of year. Thus, the survey date also provides a best-case scenario for the binary SCA mapper. If we are only interested total volume in subalpine and alpine areas, then a peak accumulation or early season survey should suffice.

If we are interested in the timing of the runoff, then we need periodic estimates of snow distribution earlier and later in the season. Peak snow melt runoff periods for most watersheds in this mountain range frequently occur while snow lies in the forested areas. As our area of interest increases in size, forested area almost inevitably increases, while the ratio of alpine to forested area decreases. Forested areas comprise the majority of early season mixed pixels, where binary mapping algorithms have difficulty producing accurate results. In the case of the Blackcap Basin, forest area increases substantially as one proceeds down the drainage, while increase in alpine area is small. As snow cover diminishes through the melt season, experience tells us that the spatial structure of the remaining snow changes, with the size of snow fields shrinking. Depending on the resolution of the digital imagery, an increasing fraction of the snow may occur in pixels less than 50% snow covered. The pathological case would be where the basin was made up of pixels with 49% snow cover. A binary mapper would theoretically map the entire basin as snow free, although it was actually nearly half covered with snow. This example represents an extreme case and is not realistic, but it does illustrate a potential source of error that would increase with decreasing snow patch size.

The methods we have described to map SWE rely on techniques not likely to become operational soon. The primary SWE interpolation requires far more data points than exist in an equivalent operational setting. Our experience with classification and regression trees shows the requirement for hundreds of samples for model stability. Likewise, the unsupervised spectral unmixing of snow fraction tested thousands of potential mixture models, which was computationally intensive. However, with the increasing demand to improve the accuracy of operational products, we point to the potential for limited experiments like we reported here to provide important data sets for both improving operational methods and learning more about the variables that affect SWE distribution at different scales.

SUMMARY

We have shown in this study that binary regression trees can interpolate measurements from a detailed snow survey of a basin with great extremes of topography, energy balance, elevation and biomes. Using point data alone the model explained 60-70% of the observed variance of SWE. Unsupervised spectral mixture analysis produced snow area estimates, on a pixel-by-pixel basis, that offer more detailed information than binary snow maps. We have shown that merging these data produced adjusted spatial estimates of SWE that are suitable for analyzing the effects of different methods and variables.

REFERENCES

Boardman, J., Automating spectral unmixing of AVIRIS data using convex geometry concepts, in *Summaries of the Fourth Annual JPL Airborne Geoscience Workshop*, vol. 1, pp. 11-14, 1993.

Breiman, L., Friedman, J., Olshen, R., and Stone, C., *Classification And Regression Trees*, Wadsworth and Brooks, Pacific Grove, CA, 1984.

California Cooperative Snow Surveys, *Bulletin 120-93, Report 4*, State of California, Department of Water Resources, Sacramento, CA, 1993.

Carroll, S. and Cressie, N., A comparison of geostatistical methodologies used to estimate snow water equivalent, *Water Resources Bulletin, 32*, 267-278, 1996.

Carroll, S., Day, G., Cressie, N., and Carroll, T., Spatial modeling of snow water equivalent using airborne and ground-based snow data, *Environmetrics, 6*, 127-139, 1995.

Carroll, T., GIS used to derive operational hydrologic products from in situ and remotely sensed snow data, in *Geographical Information Systems in Assessing Natural Hazards*, edited by A. Carrara and F. Guzzetti, pp. 335-342, Kluwer Academic Publishers, 1995.

Chambers, J. and Hastie (eds.), T., *Statistical Models in S*, Wadsworth and Brooks, Pacific Grove, CA, 1992.

Clark, L. and Pregibon, D., Tree-based models, in *Statistical Models in S*, edited by J. Chambers and T. Hastie, pp. 377-419, Wadsworth and Brooks, Pacific Grove, CA, 1992.

Dozier, J., A clear-sky spectral solar radiation model for snow-covered mountainous terrain, *Water Resources Research, 16*, 709-718, 1980.

Dozier, J., Snow reflectance from LANDSAT-4 Thematic Mapper, *IEEE Transactions on Geoscience and Remote Sensing, GE-22*, 323-328, 1984.

Dozier, J., Spectral signature of alpine snow cover from the Landsat Thematic Mapper, *Remote Sensing of Environment, 28*, 9-22, 1989.

Dozier, J. and Marks, D., Snow mapping and classification from LANDSAT Thematic Mapper data, *Annals of Glaciology, 9*, 97-103, 1987.

Elder, K., Snow Distribution in Alpine Watersheds, Ph.D. Dissertation, 309 pp., Department of Geography, University of California, Santa Barbara, 1995.

Elder, K., Dozier, J., and Michaelsen, J., Snow accumulation and distribution in an alpine watershed, *Water Resources Research, 27*, 1541-1552, 1991.

Elder, K., Michaelsen, J., and Dozier, J., and 129-139,, Small basin modeling of snow water equivalence using binary regression tree methods, in *Biogeochemistry of Seasonally Snow-Covered Areas*, IAHS-AIHS and IUGG XXI General Assembly, Boulder, Colorado, July, 1995, International Association of Hydrological Sciences, Wallingford, UK, 1995.

Frew, J. and Dozier, J., The Image Processing Workbench - portable software for remote sensing instruction and research, in *Proceedings IGARSS '86*, ESA SP-254, pp. 271-276, European Space Agency, Paris, 1986.

Hall, D., Riggs, G., and Salomonson, V., Development of methods for mapping global snow cover using Moderate Resolution Imaging Spectroradiometer data, *Remote Sensing of Environment, 54*, 127-140, 1995.

Hall, D., Riggs, G., Salomonson, V., Chien, J., Klein, A., and Moore, A., Algorithm Theoretical Basis Document (ATBD) for the MODIS Snow-, Lake Ice- and Sea Ice-Mapping Algorithms, *Version 3.0, November 1*, 1996.

Hosang, J. and Dettwiler, K., Evaluation of a water equivalent of snow cover map in a small catchment area using a geostatistical approach, *Hydrological Processes, 5*, 283-290, 1991.

Kneizys, F., Shettle, E., Abreu, L., Chetwynd, J., Anderson, G., Gallery, W., Selby, J., and Clough, S., Users Guide to LOWTRAN7, *Report AFGL-TR-88-0177*, Air Force Geophysics Laboratory, Bedford, MA, 1988.

Lawton, W. and Sylvestre, E., Self modeling curve resolution, *Technometrics, 13*, 617-633, 1971.

Lowry, S. and Huppler, D., Infrared spectral search system for gas chromatography/Fourier Transform infrared spectrometry, *Analytical Chemistry, 53*, 889-893, 1981.

Martinec, J. and Rango, A., Areal distribution of snow water equivalent evaluated by snow cover monitoring, *Water Resources Research, 17*, 1480-1488, 1981.

Maxson, R., Allen, M., and Szeliga, T., Image classification by comparison of angles created between multi-channel vectors and an empirically selected reference vector, in *1996 North American Airborne and Satellite Snow Data CD-ROM*, Chanhassen, Minnesota, 1996.

Mertes, L., Smith, M., and Adams, J., Estimating suspended sediment concentrations in surface waters of the Amazon River wetlands from Landsat images, *Remote Sensing of Environment, 43*, 281-301, 1993.

Nolin, A. and Dozier, J., Estimating snow grain size using AVIRIS data, *Remote Sensing of Environment, 44*, 231-238, 1993.

Painter, T., Roberts, D., Green, R., and Dozier, J., Subpixel snow-covered area and snow grain size from mixture analysis with AVIRIS data, in *Sixth Annual JPL Airborne Earth Science Workshop*, Jet Propulsion Laboratory, Pasadena, CA, 1996.

Rango, A. and Itten, K., Satellite potentials in snowcover monitoring and runoff prediction, *Nordic Hydrology, 7*, 209-230, 1976.

Rosenthal, W., Automated snow mapping at subpixel resolution from NOAA-AVHRR data, in *Final Report: Programs for estimating subpixel snow-covered area*, U.S. Army Cold Regions Research and Engineering Laboratory, Hanover, NH, 1996b.

Rosenthal, W., Estimating alpine snow cover with unsupervised spectral unmixing, in *Proc. IGARSS '96*, pp. 2252-2254, 1996a.

Rosenthal, W. and Dozier, J., Automated Mapping of Montane Snow Cover at Subpixel Resolution from the Landsat Thematic Mapper, *Water Resources Research, 32*, 115-130, 1996.

Satterwhite, M. and Henley, J., Hyperspectral signatures (400 to 2500 nm) of vegetation, minerals, soils, rocks, and cultural features: laboratory and field measurements, in *Technical Report ETL-0573*, U.S. Army Corps of Engineers, Engineering Topographic Laboratories, Fort Belvoir, VA, 1990.

Smith, M., Ustin, S., Adams, J., and Gillespie, A., Vegetation in deserts: 1. A regional measure of abundance from multispectral images, *Remote Sensing of Environment, 29*, 1-26, 1990.

Tanré, D., Deroo, C., Duhaut, P., Herman, M., and et al.,, Description of a computer code to simulate the satellite signal in the solar spectrum - The 5S code, *International Journal of Remote Sensing, 11*, 659-668, 1990.

Zar, J., *Biostatistical Analysis*, 2nd ed., 718 pp., Prentice-Hall, Englewood Cliffs, New Jersey, 1984.

TABLE 1.
SNOW-COVERED AREA METHOD COMPARISON

SCA method	(ha)	% basin	Δ SCA % from subpixel estimate
subpixel (0-100%)	7657	82.6	NA
binary (≥40%)	8834	95.3	13.3
binary (≥50%)	7953	87.8	3.7
binary (≥60%)	7407	79.9	-3.4

TABLE 2.
SNOW WATER EQUIVALENCE COMPARISON
RESULTING FROM DIFFERENT
SNOW-COVERED AREA METHODS

SCA method	SWE* volume (m^3)	Δ SWE from subpixel estimate (m^3)	Δ SWE % from subpixel estimate
subpixel (0-100%)	89,270,000	NA	NA
binary (≥40%)	101,000,000	11,720,000	13%
binary (≥50%)	93,700,000	4,430,000	5%
binary (≥60%)	88,700,000	-750,000	-1%

*SWE volume based on 25-node binary tree model

Figure 1. Location map of the study basin.

WESTERN
UNITED STATES

KINGS RIVER BASIN
Blackcap Basin
(inset)

Figure 2. Locations of field measurements in Blackcap basin. Small points represent depth measurements along transects; Large points represent snow pit sites or location of mean densities calculated from Mount Rose transect data.

Figure 4. Digital elevation model of the Blackcap basin. Dark areas represent low elevations; bright areas represent high elevations. The DEM is a USGS standard product and is mapped at a 30 m grid resolution. Range is 2476 m to 3827 m a.s.l.
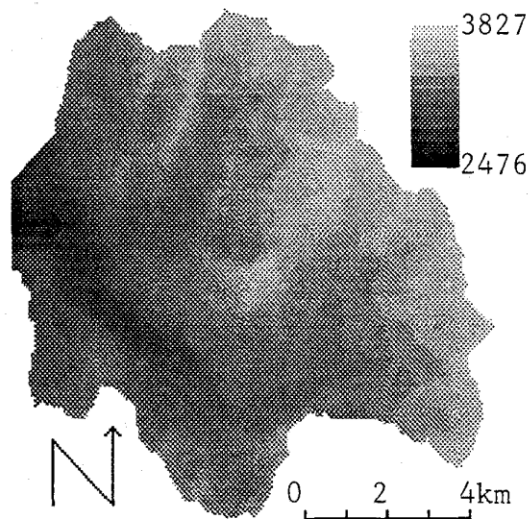

Figure 3. Calculated net radiation over the Blackcap basin. Dark areas represent low values; bright areas represent high values. Range is $7\,\mathrm{W\,m^{-2}}$ to $196\,\mathrm{W\,m^{-2}}$.

Figure 5. Slope angles in the Blackcap basin. Dark regions represent flatter areas; light areas represent steep slopes. The slope mapping was calculated from the DEM in Figure 4. Range is 0° to 58°, although actual slopes in the basin certainly reach higher values.
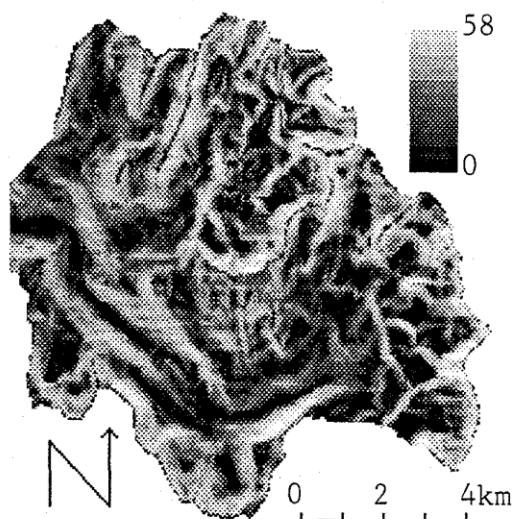
Figure 6. Twenty five node regression tree for snow depth. The values in the ellipsoidal and rectangular nodes are the mean snow depths for all points satisfying the splitting criteria leading to the node. Rectangular boxes are terminal nodes.
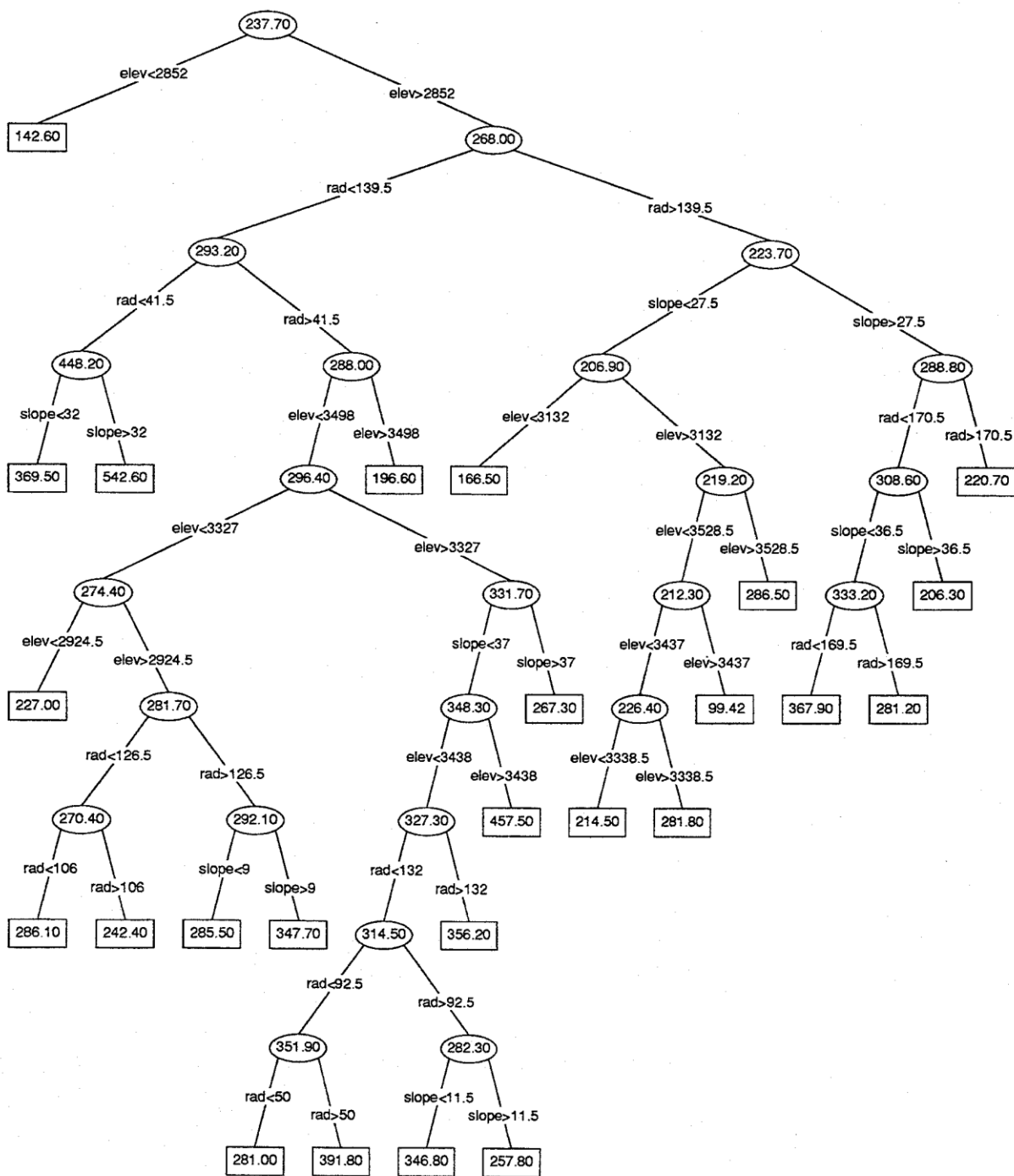
Figure 7. Snow depth mapped over the entire Blackcap basin using the regression tree shown in Figure 6. Dark areas represent low snow depth; light areas represent deep accumulations of snow. Snow-covered area is not indicated on this map; snow depth is assigned over the entire basin based on the regression tree splits. Range is 0.99 m to 5.43 m.

Figure 9. Snow density mapped over the Blackcap basin using a multiple linear regression. Dark areas represent lower mean densities; light colors represent higher mean densities. Range is $408 \, \mathrm{kg \, m^{-3}}$ to $522 \, \mathrm{kg \, m^{-3}}$.

Figure 8. Coefficient of determination for the regression trees from the underfit 2-node tree to the overfit 35 node tree.

Number of Terminal Nodes or SWE Classes
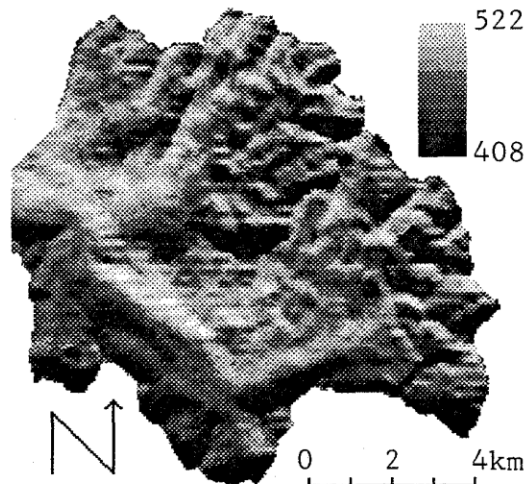
Figure 10. Subpixel fractional snow-covered area mapped over the Blackcap basin. White areas represent snow-free pixels; black areas represent 100% snow-covered pixels. Range is 0 to 100%.
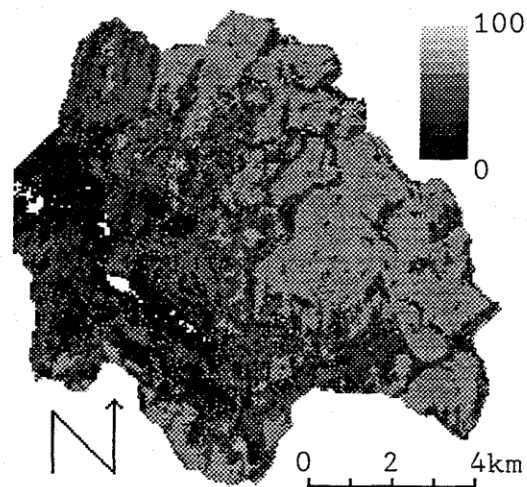

40

Figure 11. Binary mapping of snow-covered area derived from the subpixel fractional map in Figure 10. A is the 40% map where all pixels with 40% or greater SCA in Figure 10 are considered to be 100% snow covered; B is the 50% map where all pixels with 40% or greater SCA are considered to be 100% snow covered; C is the 60% map where all pixels with 60% or greater SCA are considered to be 100% snow covered. White pixels are snow-free regions; black pixels are 100% snow covered.
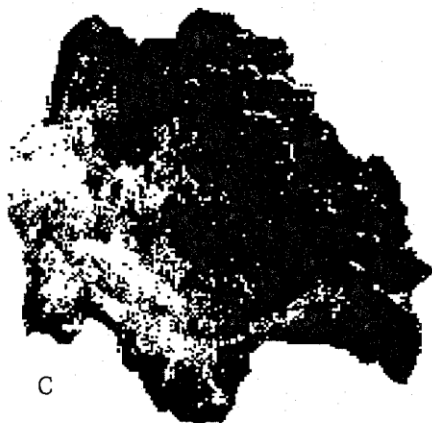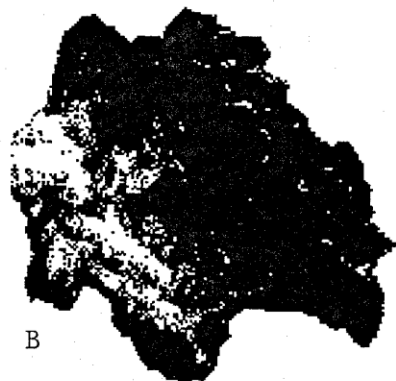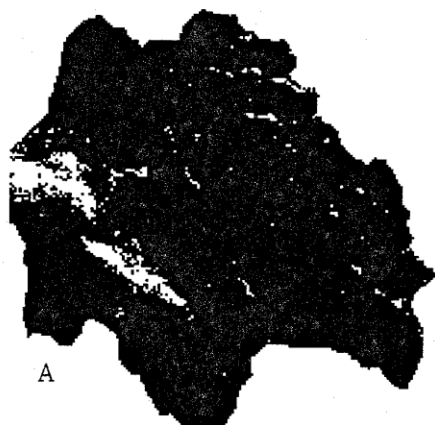
Figure 12. Areal mapping of snow water equivalence over the Blackcap basin where the snow depth mapping (Figure 7), snow density (Figure 9) and fractional snow-covered area (Figure 10) are combined. Range is 0 to 2.37 m.
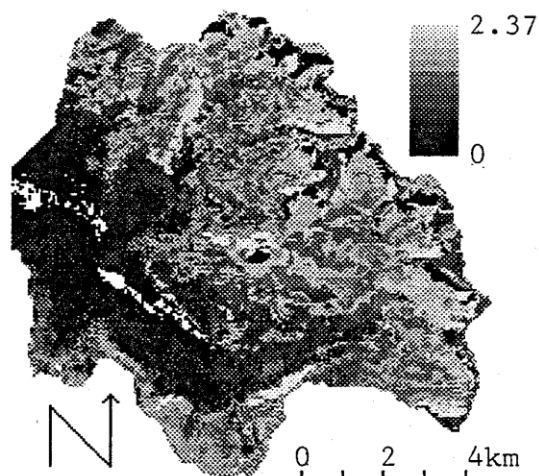

Figure 13. Histogram of percent basin area covered by a given snow cover fraction.